Research in Astron. Astrophys. **2013** Vol. **13** No. **2**, 207–214
http://www.raa-journal.org *http://www.iop.org/journals/raa*

***R**esearch in*
***A**stronomy and*
***A**strophysics*

Dynamics of neutrino-driven winds: inclusion of accurate weak interaction rates in strong magnetic fields *

Men-Quan Liu[1,2] and Zhong-Xiang Wang[1]

[1] Shanghai Astronomical Observatory, Chinese Academy of Sciences, Shanghai 200030, China; *liumq@shao.ac.cn*
[2] Institute of Theoretical Physics, China West Normal University, Nanchong 637002, China

Received 2012 July 27; accepted 2012 October 9

Abstract Solving Newtonian steady-state wind equations while considering the accurate weak interaction rates and magnetic fields (MFs) of young neutron stars, we study the dynamics and nucleosynthesis of neutrino-driven winds (NDWs) from proto neutron stars (PNSs). For a typical 1.4 $M_\odot$ PNS model, we find that the nucleosynthesis products are closely related to the luminosity of neutrinos and anti-neutrinos. The lower the luminosity is, the larger is the effect on the NDWs caused by weak interactions and MFs. At a high anti-neutrino luminosity of typically 8×10^{51} erg s^{-1}, neutrinos and anti-neutrinos dominate the processes in an NDW and the MFs hardly change the wind's properties. But at a low anti-neutrino luminosity of 10^{51} erg s^{-1} at the late stage of an NDW the mass of the product and process of nucleosynthesis are changed significantly in strong MFs. Therefore, in most of the models considered for the NDWs from PNSs, based on our calculations, the influences of MFs and the net weak interactions on the nucleosynthesis are not significant.

Key words: nuclear reactions, nucleosynthesis, abundances — hydrodynamics — stars: neutrons

1 INTRODUCTION

The neutrino-driven wind (NDW) from a proto-neutron star (PNS) was firstly proposed by Duncan et al. (1986). It has been regarded as a major candidate site for r-process nucleosynthesis according to observations of metal-poor stars in recent years (Qian 2008). A basic scenario of the r-process nucleosynthesis in an NDW can be simply described by following Martínez-Pinedo (2008). Soon after the birth of a PNS, neutrinos and anti-neutrinos are emitted from the surface of the PNS. Because of photodisintegration caused by the shock wave in the supernova explosion, the main composition of the circumstellar environment of the PNS is protons, neutrons, electrons and positrons. The main reactions are the absorption and emission of neutrinos and anti-neutrinos by nucleons (in the so called 'neutrino heat region'). At a certain distance from the PNS, electron fraction $Y_{\rm e}$ remains constant and α particles are formed. Above this region, other particles, such as ^{12}C and ^{9}Be, are

∗ Supported by the National Natural Science Foundation of China.

successively produced as seed nuclei. Abundant neutrons are captured by the seed nuclei in succession. The neutron-to-seed ratio Δn is crucial for building a successful r-element pattern, where Δn is determined by three essential parameters: electron fraction, entropy and expansion timescale.

It is difficult to obtain the parameters that fulfill all the nucleosynthesis conditions with self-consistency. Detailed analyses for NDWs have been carried out, considering Newtonian and general relativistic hydrodynamics, and physical conditions such as rotation, magnetic fields (MFs) and termination shocks (Kuroda et al. 2008; Metzger et al. 2007; Qian & Woosley 1996; Thompson 2003; Thompson et al. 2001). Among the analyses, the calculations of weak interaction rates are usually treated in an oversimplified way. It is known that young neutron stars (NSs) have a typical MF of $\sim 10^{13}$ G, and the surface MF strength of magnetars can be as large as 10^{15} G (Woods & Thompson 2006). Strong MFs can potentially change the weak interaction rates significantly. The weak interaction rates decide the electron fraction in the wind, and are very important for the final r-process or νp-process nucleosynthesis. For example, Wanajo et al. (2009) have shown that the puzzling excess of r-element $A = 90$ may be solved if $Y_{\rm e}$ is increased by 1%–2%. Recently, Arcones & Martínez-Pinedo (2011) considered the precise weak interaction rates but without MFs. In this paper, we report our work of investigating the NDW in detail considering the accurate weak interaction rates in strong MFs, which is more realistic and practical.

2 MODELS

2.1 Dynamic Equations of NDWs

It has been shown that the steady state is a good approximation for an NDW in the first 20 seconds (Qian & Woosley 1996; Thompson 2003; Thompson et al. 2001). Evolution of the wind is usually obtained by solving the differential equations that include hydrodynamic equations, the equation of state (EoS) and neutrino reaction rates. The dynamical equations of an NDW with the MF pressure are given as follows (Qian & Woosley 1996):

$$4\pi r^2 \rho v = \dot{M}, \tag{1}$$

$$v\frac{dv}{dr} = -\frac{1}{\rho}\frac{dP}{dr} - \frac{GM}{r^2}, \tag{2}$$

$$v\frac{d\varepsilon}{dr} - \frac{v}{\rho^2}P\frac{d\rho}{dr} = \dot{q}, \tag{3}$$

$$v\frac{dY_{\rm e}}{dr} = \lambda^B_{\nu_{\rm e}n} + \lambda^B_{{\rm e}^+n} - (\lambda^B_{\nu_{\rm e}n} + \lambda^B_{{\rm e}^+n} + \lambda^B_{\bar{\nu}_{\rm e}p} + \lambda^B_{{\rm e}^-p})Y_{\rm e}, \tag{4}$$

$$P = \frac{11\pi^2}{180}\frac{k^4}{(\hbar c)^3}\Big(1 + \frac{30\eta^2}{11\pi^2} + \frac{15\eta^4}{11\pi^4}\Big)T^4 + \frac{k}{m_N}\rho T + \frac{B^2}{8\pi}. \tag{5}$$

Here Equation (1) denotes the mass conservation, where r is the distance from the PNS center to the wind, v is the velocity and $\dot{M}$ is the outflow rate per second. Equation (2) denotes the dynamic equilibrium, where G is the gravitational constant and M is the mass of the PNS. Equation (3) denotes the energy conservation, where

$$\varepsilon = \frac{11\pi^2}{60\rho}\frac{k^4}{(\hbar c)^3}\Big(1 + \frac{30\eta^2}{11\pi^2} + \frac{15\eta^4}{11\pi^4}\Big)T^4 + \frac{3}{2}\frac{k}{m_N}T$$

is the internal energy, k is Boltzmann's constant, $\eta \equiv \mu_{\rm e}/kT$ is the degeneracy parameter, $\mu_{\rm e}$ is the electron chemical potential, and $\dot{q}$ is the total net heating rate for each nucleon (i.e., specific heating rate), and can be divided to two parts: heating and cooling. Detailed calculations of $\dot{q}$ can be found in Qian & Woosley (1996). Equation (4) denotes the equilibrium of the composition, that is to say, the

change of electrons must be balanced with the variations of the electron fraction, where $\lambda^B_{\rm parameters}$ represent a variety of weak interaction rates in MFs like those listed in Equation (4). The subscripts of $\lambda^B_{\rm parameters}$ denote the particles participating in the reaction. Equation (5) is the EoS, in which $\hbar$ is the Planck constant and c is the speed of light. Equation (5) can be decomposed into three parts:

$$\frac{\pi^2}{45}\frac{k^4}{(\hbar c)^3}T^4, \quad \frac{7\pi^2}{180}\frac{k^4}{(\hbar c)^3}T^4+\frac{\eta^2}{6}\frac{k^4}{(\hbar c)^3}T^4+\frac{\eta^4}{12\pi^2}\frac{k^4}{(\hbar c)^3}T^4 \quad \text{and} \quad B^2/8\pi.$$

They represent the pressure of photons, electron-positron pairs and MFs, respectively. In the EoS, we adopted the assumption given by Cooper & Kaplan (2010): the nonradial (e.g., toroidal) component of the MF is large compared to its radial component. We set the MF as a dipole field: $B(r) = B_i(\frac{R_i}{r})^3$, where R_i and B_i are the radius and the surface MF strength of the PNS respectively. The radius of the PNS was set to be 10 km.

2.2 Boundary Conditions and Numerical Techniques

We considered a typical PNS model with a baryonic mass of $1.4\,M_\odot$, obtained in a spherically symmetric simulation of a parameterized $15\,M_\odot$ supernova explosion model. Detailed simulations showed that there are a few α particles appearing at the neutrino sphere, but the number density of α particles is much smaller than those of protons and neutrons (Arcones et al. 2008). As a result, it was reasonable to ignore the influence of α particles on the electron fraction. The initial conditions and neutrino and anti-neutrino luminosities we chose were the same to those in Thompson et al. (2001): boundary temperature $T_i = 4.3427\times10^{10}$ K, density $\rho_i = 1{\times}10^{13}$ g cm^{-3} and electron fraction $Y_{\rm ei} = 0.03$. Two anti-neutrino luminosity models were considered. For anti-neutrino luminosity $L_{\bar\nu_{\rm e}} = 8{\times}10^{51}$ erg s^{-1}, we adopted

$$\begin{aligned} L_{\nu_{\rm e}} &= 6.15\times10^{51}\,{\rm erg\,s^{-1}}, \quad L_{\nu_\mu} = 5.71\times10^{51}\,{\rm erg\,s^{-1}},\\ E_{\nu_{\rm e}} &= 11\,{\rm MeV}, \quad E_{\bar\nu_{\rm e}} = 14\,{\rm MeV} \qquad \text{and} \qquad E_{\nu_\mu} = 23\,{\rm MeV}. \end{aligned}$$

For anti-neutrino luminosity $L_{\bar\nu_{\rm e}} = 1{\times}10^{51}$ erg s^{-1}, we adopted

$$\begin{aligned} L_{\nu_{\rm e}} &= 7.69\times10^{50}\,{\rm erg\,s^{-1}}, \quad L_{\nu_\mu} = 7.14\times10^{50}\,{\rm erg\,s^{-1}},\\ E_{\nu_{\rm e}} &= 6.54\,{\rm MeV}, \qquad E_{\bar\nu_{\rm e}} = 8.32\,{\rm MeV} \quad \text{and} \quad E_{\nu_\mu} = 13.68\,{\rm MeV}. \end{aligned}$$

We solved Equations (1)–(5) by using the Runge-Kutta method with Equations (1)–(3) rearranged to be two explicit differential equations of ρ and T. It can be noted that if the outflow mass $\dot{M}$ is given, Equations (1)–(5) are self-contained, and $\dot{M}$ is kept as a constant during the process of finding the solution. Many attempts have to be made to find a suitable $\dot{M}$ value for a cross-sonic solution in our derivation. This is because if $\dot{M}$ is too low, the speed of the wind is always lower than the local speed of sound: the wind material will accumulate at a distance not far from the PNS and the wind cannot last. For the opposite case, too large $\dot{M}$ will result in an unphysical infinite acceleration.

Because the parameters, such as ρ, vary very quickly near the PNS, the step in solving the equations is required to be sufficiently small in order to keep those parameters changing smoothly, consistent with a physical meaning. Our initial step was usually less than 10^{-4} cm, but it was adjusted automatically in our code by assuming that the values of all parameters increased in steps that were not more than 0.01 of themselves. It is complicated to calculate the electron chemical potentials and weak interaction rates in strong MFs because many integrals and accumulations must be calculated iteratively and the step must be very small as mentioned above. Hence we first obtained the database for the electron chemical potentials and weak interaction rates in the physical environments of the winds, and used their interpolated values during the processes of solving the wind equations.

2.3 Influences of MFs

The existence of an MF not only affects the pressure, but also the electron chemical potentials and weak interaction rates. The main influences of the MF on the electron chemical potentials and weak interactions are phase space integrals. In free electron gas, the electron motion perpendicular to an MF is completely determined by the MF and quantized into the well-known Landau orbitals. The usual sum over electron states (per unit volume) should thus be replaced by the sum of electron states at different energy eigenstates (see e.g., Yuan & Zhang 1998). The details of how to calculate the electron chemical potentials in a strong MF can be found in Zhang et al. (2010). Basically, the number of states for electrons in an MF at momentum interval $[p_z \rightarrow p_z + dp_z]$ is proportional to the MF strength, i.e., $\frac{eB}{(2\pi\hbar)^2 c} dp_z$, where e and p_z are the charge and momentum of electrons along the MF respectively. The number of microstates for electrons in the unit volume is equal to the number density of electrons, so for a given number density of electrons, the increase of the MF will reduce the effective integral interval of dp_z, as well as the electron chemical potentials. In other words, the MF provides a new state parameter compared to that without the MF, and increases the state density in the phase space. In the actual numerical calculations, due to the abrupt transitions between the quantized Landau levels in the plane perpendicular to the MF, there may be gurgitation (see Fig. 1), but the electron chemical potentials generally decrease when subjected to MFs.

Fassio-Canuto first investigated the β decay of free neutrons in strong MFs (Fassio-Canuto 1969). Later, many authors developed the weak interaction calculations in strong MFs (e.g., Lai & Qian 1998; Luo & Peng 1997; Duan & Qian 2005). Generally, the effect of an MF on a transition matrix element can be ignored when compared to the effect of an MF on phase space. There are mainly four types of weak interactions (including their forward and reverse reactions) in NDWs $\nu_{\rm e} + n \Leftrightarrow {\rm e}^- + p$ and $\bar{\nu}_{\rm e} + p \Leftrightarrow {\rm e}^+ + n$. For the neutrino and anti-neutrino absorption reactions, described by $\nu_{\rm e} + n \rightarrow {\rm e}^- + p$ and $\bar{\nu}_{\rm e} + p \rightarrow {\rm e}^+ + n$, we adopted the method of Lai & Shapiro (1991), in which both the MF and thermal motion of nucleons were considered. Since the energies of neutrinos and anti-neutrinos are very large (more than 10 MeV for $L_{\bar{\nu}_{\rm e}} = 8\times10^{51}$ erg s^{-1}), the cross sections change slightly [as shown in figs. 1, 2 and 3 in Lai & Shapiro (1991)]. As for the electron and positron capture rates ${\rm e}^- + p \rightarrow \nu_{\rm e} + n$ and ${\rm e}^+ + n \rightarrow \bar{\nu}_{\rm e} + p$, we used the method of Luo &

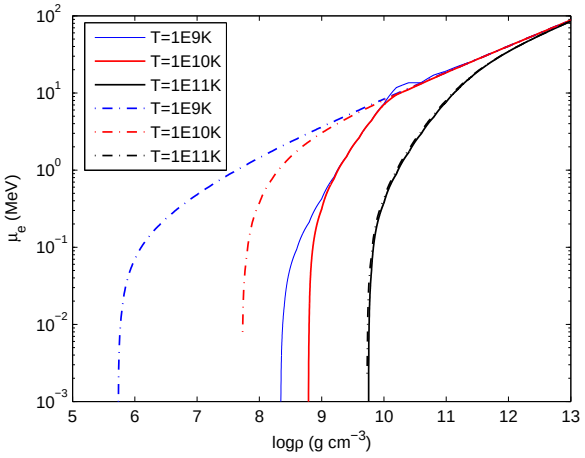

Fig. 1 The electron chemical potentials (without rest mass) as a function of density at different temperatures. Solid and solid-dotted curves indicate the potentials with $B = 0$ and $B = 10^{15}$ G, respectively.

Table 1 The Weak Interaction Rates at the Critical Radius of Weak Interaction Freeze-out (T=10^{10} K)

Model	$\log_{10} B$(G)	R_{cr}(cm) ($\times 10^6$)	$\lambda^B_{e^-p}$ (s^{-1}) ($\times 10^{-2}$)	$\lambda^B_{e^+n}$ (s^{-1}) ($\times 10^{-1}$)	$\lambda^B_{\bar{\nu}_e n}$($s^{-1}$)	$\lambda^B_{\nu_e p}$(s^{-1})	Y_e ($\times 10^{-1}$)
$L_{\bar{\nu}_e,51}=1$	13	2.16	9.15	3.59	7.21	5.81	5.62
	14	2.23	9.17	3.58	6.80	5.48	5.62
	15	3.85	9.57	3.44	2.27	1.83	5.76
$L_{\bar{\nu}_e,51}=8$	13	3.85	9.39	3.50	26.7	28.5	4.86
	14	3.87	9.40	3.50	26.4	28.2	4.86
	15	4.79	9.60	3.43	17.2	18.4	4.87

Notes: $L_{\bar{\nu}_e,51}$ denotes the luminosity in the units of 10^{51} erg s^{-1}.

Peng (1997) and Duan & Qian (2005). An MF larger than the critical MF ($B_{\rm cr} = 4.4\times10^{13}$ G) can make the rates change dramatically. The lower the positron/electron energy is, the more easily the phase space distribution of the positron/electron can be changed.

3 RESULTS AND DISCUSSION

The results of the electron chemical potentials as a function of density at different temperatures and MFs are shown in Figure 1. The MF strengths considered were 0, 10^{13}, 10^{14} and 10^{15} G. Compared to that without an MF, there are obvious changes of the electron chemical potentials for the MF $B = 10^{15}$ G at low temperatures ($T < 10^{10}$ K) and low densities ($\rho Y_{\rm e} < 10^9$ g cm^{-3}). However when the MF is lower than 10^{15} G, such as 10^{13} and 10^{14} G, no significant differences are found. Actually because the curves for such low MFs nearly coincide with those without an MF, they are not shown in Figure 1. In addition, as the temperature near the PNS is very high (more than 10^{10} K), the changes of the electron chemical potentials near the surface of the PNS are also not significant.

Referring to Equations (4) and (5), the electron chemical potentials can change the degenerate parameter and EoS, and the weak interaction rates determine the change of $Y_{\rm e}$.

In Table 1, the results at the critical radius of weak interaction freeze-out are given, at which the final $Y_{\rm e}$ values were also obtained (Martínez-Pinedo 2008). We found that the electron and positron capture rates in the strong MFs can change the $Y_{\rm e}$ distribution near the surface of the PNS, but hardly change the final $Y_{\rm e}$ of nucleosynthesis. This is because, although an MF larger than the critical MF can make the electron/positron capture rates greatly change, the capture rates are generally much less important than neutrino and anti-neutrino absorption rates due to the high energy and luminosity of neutrinos and anti-neutrinos. In addition, the MF strength near the PNS in our dipole model decreases very quickly as the radius increases. For example, for the surface MF strength of the PNS of 10^{15} G, it decreases to 3.7×10^{13} G at a radius of 30 km, which is already below the critical MF.

The obtained properties of the NDW are shown in Figures 2 ($L_{\bar{\nu}_e} = 8\times10^{51}$ erg s^{-1}) and 3 ($L_{\bar{\nu}_e} = 10^{51}$ erg s^{-1}). As can be seen, the larger the luminosity of anti-neutrinos is, the smaller the change will be. The reason for this is that the pressure mainly depends on the absorption rates of neutrinos and anti-neutrinos, which are a function of luminosity and average energy of neutrinos and anti-neutrinos. In the high luminosity condition, the MF causes little difference, but for the low luminosity, the case reverses. Although the trends of all parameters, density, temperature, and entropy, are the same, some differences are clearly visible. The density near the PNS shows a large decrease by several orders of magnitude, but drops relatively slowly for the higher anti-neutrino luminosity and stronger MF. Compared to the density, the temperature decreases as a function of the radius much more gently, by a factor < 5 at radius $R = 20$ km. The MF and weak interaction rates influence the heating rates, lowering the nucleon entropy, especially for the low anti-neutrino

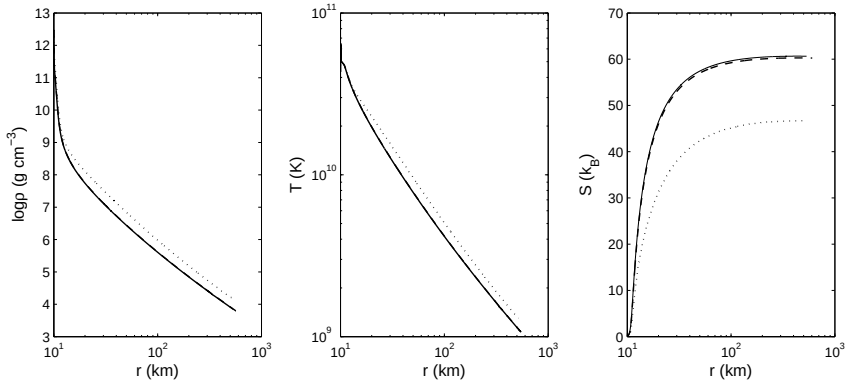

Fig. 2 The density, temperature and entropy as a function of radius for $L_{\bar{\nu}_e} = 8 \times 10^{51}$ erg s^{-1}. The solid, dashed and dotted lines indicate the results of $B = 1 \times 10^{13}$, $1{\times}10^{14}$ and $1{\times}10^{15}$ G, respectively.

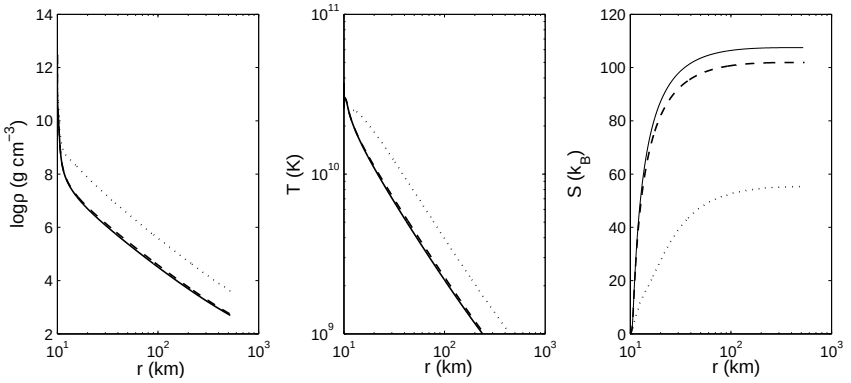

Fig. 3 The density, temperature and entropy as a function of radius for $L_{\bar{\nu}_e}$=$1{\times}10^{51}$ erg s^{-1}. Descriptions of lines are the same as in Fig. 2.

luminosity and strong MF case (right panel of Fig. 3). Based on the results obtained, we conclude that the density and temperature in our dynamical models have relatively small changes when the MFs are considered, but the variation of nucleon entropy under the influence of a strong MF is significant, which affects the result of nucleosynthesis accordingly.

In Table 2 a summary of our model calculations is given based on the method described in Roberts et al. (2010). As can be seen, the mass outflow rate increases with the anti-neutrino luminosity, and the MF enhances the total mass of the NDW. r-element distribution patterns depend on the entropy, expansion timescale and electron fraction. For the nucleon entropy, we found that it changes to be smaller under the strong MFs, which is caused by the difference of heating rate and heating timescale. For the expansion timescale τ_d, we used the definition of Metzger et al. (2007), and our results show that in the MF $B = 10^{15}$ G, the expansion timescale is much larger than the others. As for the electron fraction, it remains nearly the same even under the ultra-strong MF for high anti-neutrino luminosity.

For model $L_{\bar{\nu}_e,51} = 8$, $Y_e = 0.486$, which implies there is a neutrino-rich wind, the r-process nucleosynthesis begins after the charged particle reactions occur, and the total quantity of nucleosyn-

Table 2 Nucleosynthesis Parameters Resulting from Our Models

Model	$\log_{10}B$ (G)	$\dot{M}$ ($M_\odot$ s^{-1})	$S(k)$	τ_d (ms)	$Y_{\rm e}$	Y_s ($\times10^{-3}$)	Δ_n
$L_{\bar{\nu}_{\rm e},51}=8$	13	2.40×10^{-4}	60.66	10.55	0.486	2.76	10.13
	14	2.41×10^{-4}	60.28	10.73	0.486	2.77	10.11
	15	3.53×10^{-4}	46.70	18.22	0.487	2.60	10.00
$L_{\bar{\nu}_{\rm e},51}=1$	13	1.58×10^{-6}	107.50	123.62	0.562	1.86	1.815
	14	1.65×10^{-6}	101.90	143.76	0.562	2.29	1.569
	15	5.47×10^{-6}	55.3	469.86	0.576	8.30	0.440

thesis is determined by the outflow mass. It can be seen from Table 2 that the mass outflow rate with the MF of $B=10^{15}$ G is increased by about 1/3, and the changes of S and τ_d are also significant for the case $B=10^{15}$ G. However, the differences in seed nuclei abundance Y_s and neutron-to-seed ratio Δ_n at different MFs are very small.

The reasons for this are the following. In the stage of charged particle reactions, high entropy will effectively reduce the production rate of ^{12}C, because high entropy values mean more photons and thus photodisintegration becomes faster. We note that since the nuclear reaction that generates ^{12}C is the slowest in the process of generating seed nuclei, the number of ^{12}C is approximately equal to the number of seed nuclei. On the other hand, the slower the expansion is, the more slowly the density reduces. Since ^{12}C is produced by a three-body reaction, whose rate is proportional to the square of density, the increased expansion timescale increases the production of ^{12}C (Martínez-Pinedo 2008). For our results, we found that the entropy decreases significantly, and the expansion timescale also increases for the strongest MF case. Combing these two factors, for the same $Y_{\rm e}$, the seed nuclei abundance Y_s should be increased. However, the differences in the obtained Y_s are very small (Table 2). This is because the entropy is not large enough to affect Y_s, as $Y_s \approx (0.1-0.2Y_{\rm e})\times[1-\exp(-8\times10^8\tau_d S_f^{-3}Y_{\rm e}^3)]$ (Roberts et al. 2010). The change of Y_s is only sensitive to the parameters when the entropy is greater than 70. The abundance of free neutrons compared to seed nuclei is closely dependent on Y_s, and thus Δ_n also experiences small changes.

For model $L_{\bar{\nu}_{\rm e},51}=1$, $Y_{\rm e}>0.5$, which means the wind is proton-rich. For convenience of discussion, the nucleosyhthesis can be separated into two phases. During the first phase, the rapid proton capture process similar to that in Type I X-ray bursts will take place and end at the heavy nuclei with a long half-life such as ^{64}Ge. These nuclei are prohibited from capturing protons and are the seed nuclei in the second phase. During the second phase, a large number of the anti-neutrinos are continuously absorbed by protons and produce neutrons (the so called νp process). The number density of neutrons can reach 10^{14}–10^{15} cm^{-3}. These neutrons, not affected by the Coulomb repulsion, are easily captured by the seed nuclei through a series of (n, p) (p, γ) reactions to produce heavier nuclei, effectively through nuclei with a long half-life (Fröhlich et al. 2006). Therefore in an NDW, the abundance of free neutrons is essential to the final products. Based on the rough considerations (Pruet et al. 2006), the relative abundance of nucleosynthesis is proportional to $\mathrm{e}^{-\Delta_n}$, and the relative abundances were estimated to be 0.1665, 0.2122 and 0.6608 for $B=10^{13}$, 10^{14}, and 10^{15} G in our model, respectively. This implies that the yield of the νp-process is significantly increased in the strong MFs.

In this paper, using the classic calculation methods of weak interactions and electron chemical potentials, both the accurate weak interaction rates and influences of strong MFs were considered for the NDW from a PNS. We also estimated the nucleosynthesis for two cases: being neutron-rich and proton-rich, by employing analytic methods. We found that neutrino and anti-neutrino luminosities are important factors for the results. For a high luminosity case the influence of a strong MF is

small because the effect of neutrinos dominates. We note that at the late stage of an NDW when the neutrino luminosity will be relatively low, the nucleosynthesis of the νp-process in strong MFs can change significantly. For example, if the model luminosity of an anti-neutrino is 10^{50} erg s^{-1}, the entropies will be 199 k and 77 k for $B = 10^{13}$ G and 10^{15} G respectively. The difference is a factor of 2.6. The outflow rates will be $7.0 \times 10^{-9}\, M_\odot$ s^{-1} for $B = 10^{13}$ G and $3.55 \times 10^{-8}\, M_\odot$ s^{-1} for $B = 10^{15}$ G, which means the yield in the stronger MF is about five times larger than that in the lower one. However because the yield at this late stage is much lower than that in the early stage when the neutrino luminosity is high, the influence of MFs on the total yield is not significant.

Acknowledgements This work is supported by the National Natural Science Foundation of China (Grant Nos. 11073042, 11273020), the National Basic Research Program of China (973 Project, 2009CB824800), China Postdoctoral Science Foundation funded project (2012T50446), the Fund of Sichuan Provincial Education Department (10ZC014), and the Science and Technological Foundation of CWNU (11B008). ZW is a Research Fellow of the One-Hundred Talents project of Chinese Academy of Sciences.

References

Arcones, A., & Martínez-Pinedo, G. 2011, Phys. Rev. C, 83, 045809
Arcones, A., Martínez-Pinedo, G., O'Connor, E., et al. 2008, Phys. Rev. C, 78, 015806
Cooper, R. L., & Kaplan, D. L. 2010, ApJ, 708, L80
Duan, H., & Qian, Y.-Z. 2005, Phys. Rev. D, 72, 023005
Duncan, R. C., Shapiro, S. L., & Wasserman, I. 1986, ApJ, 309, 141
Fassio-Canuto, L. 1969, Physical Review, 187, 2141
Fröhlich, C., Martínez-Pinedo, G., Liebendörfer, M., et al. 2006, Physical Review Letters, 96, 142502
Kuroda, T., Wanajo, S., & Nomoto, K. 2008, ApJ, 672, 1068
Lai, D., & Qian, Y.-Z. 1998, ApJ, 505, 844
Lai, D., & Shapiro, S. L. 1991, ApJ, 383, 745
Luo, Z.-Q., & Peng, Q.-H. 1997, Chinese Astronomy and Astrophysics, 21, 254
Martínez-Pinedo, G. 2008, European Physical Journal Special Topics, 156, 123
Metzger, B. D., Thompson, T. A., & Quataert, E. 2007, ApJ, 659, 561
Pruet, J., Hoffman, R. D., Woosley, S. E., et al. 2006, ApJ, 644, 1028
Qian, Y. Z. 2008, in Proceedings of Science the 10th Symposium on Nuclei in the Cosmos (Michigan, USA), 1
Qian, Y.-Z., & Woosley, S. E. 1996, ApJ, 471, 331
Roberts, L. F., Woosley, S. E., & Hoffman, R. D. 2010, ApJ, 722, 954
Thompson, T. A. 2003, ApJ, 585, L33
Thompson, T. A., Burrows, A., & Meyer, B. S. 2001, ApJ, 562, 887
Wanajo, S., Nomoto, K., Janka, H.-T., Kitaura, F. S., & Müller, B. 2009, ApJ, 695, 208
Woods, P. M., & Thompson, C. 2006, Soft Gamma Repeaters and Anomalous X-ray Pulsars: Magnetar Candidates, in Compact Stellar X-ray Sources, ed. L. Walter (Cambridge Univ. Press), 547
Yuan, Y. F., & Zhang, J. L. 1998, A&A, 335, 969
Zhang, J., Wang, S.-F., & Liu, M.-Q. 2010, International Journal of Modern Physics E, 19, 437